Development of Mixed-Conducting Ceramic Membranes for Converting Methane to Syngas

U. Balachandran, P. S. Maiya, B. Ma, J. T. Dusek, R. L. Mieville, and J. J. Picciolo

Energy Technology Division
Argonne National Laboratory
Argonne, Illinois 60439 USA

April 1997

For presentation at ESF Network on Catalytic Membrane Reactors and publication in Proceedings, 4th Workshop, Oslo, Norway, May 30 - June 1, 1997.

*This work was supported by the U.S. Department of Energy, Federal Energy Technology Center, under Contract W-31-109-Eng-38.

Development of Mixed-Conducting Ceramic Membranes for Converting Methane to Syngas

U. Balachandran, P. S. Maiya, B. Ma, J. T. Dusek, R. L. Mieville, and J. J. Picciolo

Energy Technology Division
Argonne National Laboratory
Argonne, Illinois 60439 USA

Abstract

The abundantly available natural gas (mostly methane) discovered in remote areas has stimulated considerable research on upgrading this gas to high-value-added clean-burning fuels such as dimethyl ether and alcohols and to pollution-fighting additives. Of the two routes to convert methane to valuable products direct and indirect, the direct route involving partial oxidation of methane to syngas ($CO + H_2$) by air is preferred. Syngas is the key intermediate product used to form a variety of petrochemicals and transportation fuels. This paper is concerned with the selective transport of oxygen from air for converting methane to syngas by means of a mixed-conducting ceramic oxide membrane prepared from Sr-Fe-Co-O oxide. While both perovskite and nonperovskite type Sr-Fe-Co-O oxides permeate large amounts of oxygen when the membrane tube is subjected to oxygen pressure gradients, our work shows that the nonperovskite $SrFeCo_{0.5}O_x$ exhibits remarkable stability during oxygen permeation. More particularly, extruded and sintered tubes from $SrFeCo_{0.5}O_x$ have been evaluated in a reactor operating at ≈850°C for conversion of methane into syngas ($CO + H_2$) in the presence of a reforming catalyst. Methane conversion efficiencies of ≈99% were observed. In addition, oxygen permeability of $SrFeCo_{0.5}O_x$ was measured as a function of oxygen partial pressure gradient and temperature in a gas-tight electrochemical cell. Oxygen permeability has also been calculated from conductivity data and the results are compared and discussed.

1. Introduction

Conversion of natural gas (mostly methane) to more valuable liquid products such as transportation fuels and chemicals is driven by the abundance of this resource especially in remote areas. Many remote natural gas fields throughout the world remained capped because there is no market to economically utilize this resource. The conventional route is to transport the natural gas by either pipeline or as liquefied natural gas. Pipelines are economical only when the gas field is close to the gas consumer, and liquefied natural gas can be considered only on a commercial scale.

The remaining alternative is to convert natural gas by oxidation through direct or indirect technologies [1,2]. These technologies are currently used in the chemical industry to produce such basic chemicals such as ammonia, hydrogen, and methanol, which are more valuable in the market than fuel-grade products.

Product yields are low in the direct routes because the main feedstock (methane) is less reactive than the products of any upgrading process [3]. Syngas ($CO + H_2$) is the key intermediate product in the indirect route and is used to form a variety of petrochemicals and transportation

fuels. However, the cost of manufacturing syngas constitutes a large fraction of the cost of the final product. The challenge is to reduce the cost.

Two ways of producing syngas from methane are partial oxidation or steam reforming. The major cost in the partial oxidation process is for separating O_2 from N_2. Steam reforming is a highly endothermic process, and its high energy costs make it commercially unattractive [4]. This paper is concerned with a new technology that can lower the cost by using dense ceramic membranes that selectively transport oxygen from air for methane-conversion reactions.

Certain ceramic materials exhibit both electronic and ionic conductivities (of particular interest is oxygen-ion conductivity) [5-11]. These materials transport not only oxygen ions (functioning as selective oxygen separators) to the methane side (reducing) but also electrons back from the methane side to the air side (oxidizing). No external electrodes are required and if the driving force for transport is sufficient, the partial oxidation reactions should be spontaneous. Such a system will operate without an externally applied potential. Oxygen is transported across the ceramic material in the form of oxygen ions, not oxygen molecules.

The mixed-oxide conductors find other wide applications in high-temperature solid-state electrochemical devices such as solid-oxide fuel cells, batteries, and sensors. But this paper is concerned with their particular promise as ceramic membranes designed to separate oxygen from air because of their imperviousness to other gas constituents such as N_2. The separated oxygen is allowed to react with the natural gas to produce syngas in the presence of a reforming catalyst. Of course, higher oxygen ionic conductivity is desirable in the separation process.

Several perovskites based on the system $(La,Sr)(Fe,Co)O_x$ have been shown by Teraoka et al. [5-7] to exhibit not only mixed (electronic and ionic) conductivities but also appreciable oxygen permeability (two orders of magnitude higher than that of stabilized zirconia at 800°C). Many of the perovskites that we have tested in our study are not stable under methane-conversion conditions. Therefore, we have focused our research on the nonperovskite $SrFeCo_{0.5}O_x$ designated as SFC-2 [12,13]. Our reactor experiments on syngas production using extruded and sintered membrane tubes at ≈850°C are described. Finally, in-reactor oxygen permeability results are compared with those obtained from out-of-reactor experiments in an electrochemical cell where no syngas is produced and with those calculated from conductivity data.

2. Materials and Experimental Procedures

In the preparation of SFC-2, appropriate amounts of $SrCO_3$, $Co(NO_3)_2 \cdot 6H_2O$, and Fe_2O_3 were mixed and milled in isopropanol with ZrO_2 media for ≈15 h, with intermittent grinding. When dry, the mixtures were calcined in air at ≈850°C for 16 h, with intermittent grinding. After final calcination, we ground the powder with an agate mortar and pestle to an average particle size of ≈7 μm. The resulting powders were characterized by X-ray diffraction (XRD), scanning electron microscopy (SEM), and thermal analysis, and analyzed for particle-size distribution.

A slip was made from the SFC-2 powder with a solvent, dispersant, binder, and a plasticizer. The role of each additive has been described in an earlier publication [8]. Membrane tubes were fabricated by extruding the slip to an outside diameter of ≈6.5 mm, lengths up to ≈30 cm, and wall thicknesses of 0.25–1.2 mm. The extruded tubes were sintered first in air, followed by heat treatment in N_2 at ≥1100°C to achieve >90% of theoretical density and optimal mechanical properties.

The extruded and sintered tubes were characterized by SEM and XRD and used in our partial-oxidation studies to transport oxygen for the generation of syngas. Sintered rectangular bar samples were used to measure mechanical properties while sintered pellet samples were prepared for conductivity and other measurements.

The tubes were evaluated for performance in a quartz reactor system, shown in Fig. 1. Briefly, the quartz reactor supports the ceramic membrane tube with hot Pyrex seals. This design allows the ceramic tube to be in an isothermal environment. To facilitate reactions and equilibrium in the reactor, an Rh-based reforming catalyst (≈1 cm^3, 1.25 cm long, 0.2 cm wide) is loaded adjacent to the tube. A gold wire mesh wire is wrapped around the tube to prevent solid-state reactions between the catalyst and the ceramic. Both the feed gas (generally 80% methane, 20% argon) and the effluents were analyzed by gas chromatography.

Mechanical properties of the finished material were measured by conventional methods, i.e., bulk density was measured by the Archimedes principle; flexural strength, in a four-point bending mode; fracture toughness, by a single-edge notch method [14]; and Young's modulus, shear modulus, and Poisson ratio, by ultrasonic methods [15]. The thermal expansion coefficient was measured in a dilatometer.

Conductivities were measured by the conventional electron blocking four-probe method; a blocking electrode of yttria-stabilized zirconia (YSZ) was used for the oxygen ion conduction. The oxygen diffusion coefficient was measured by the conductivity relaxation method [13]. The sample was subjected to a sudden change in oxygen partial pressure pO_2, and conductivity was monitored as a function of time and temperature. Electrical conductivity measurements were also carried out inside a gas-tight electrochemical cell to determine dependence on pO_2, which in turn enabled calculation of oxygen permeability. Oxygen permeability in oxygen pressure gradients was also measured in an electrochemical cell similar to that employed for the conductivity measurements reported earlier [16]. Flowing air was used as the reference environment. Figure 2 is a schematic drawing of the gas-tight electrochemical cell used to achieve reduced pO_2 environments [17]. The specimen disk was polished to the appropriate thickness and the cylindrical side surface of the specimen disk was covered with Pyrex glass to prevent oxygen from

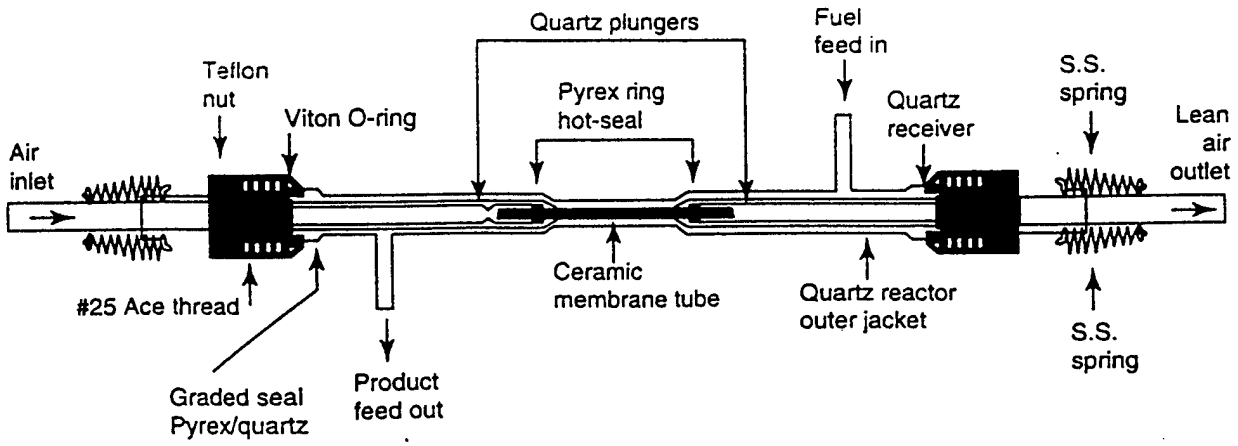

Fig. 1. Schematic diagram of ceramic membrane reactor (SS = stainless steel).

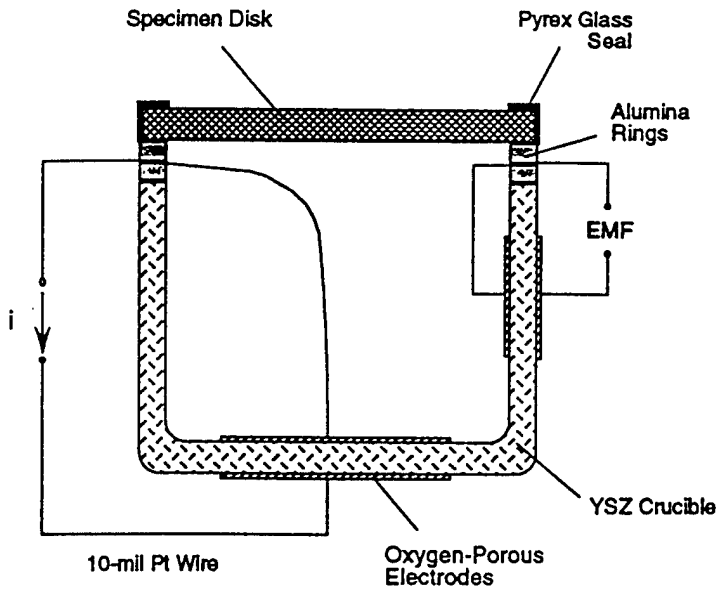

Fig. 2.
Schematic drawing of cross section of gas-tight electrochemical cell used to measure oxygen permeability in oxygen pressure gradient (YSZ = yttria stabilized zirconia).

entering the specimen through that surface. Two oxygen-porous electrodes were placed on the flat-base YSZ crucible. The bottom electrode is used to pump oxygen from the cell, while the other electrode detects the electromotive force (EMF) generated by the YSZ due to difference in pO_2. Two alumina rings were used for electrical insulation at high temperatures. The cell was sealed with Pyrex glass. Oxygen permeability was determined in the presence of a steady flow of oxygen through the specimen disk.

3. Results and Discussion

The structure of SFC-2 in 1 and 20% O_2 is shown in Fig. 3. To demonstrate the stability of this material, the structure of SFC-1 (perovskite $Sr_{0.2}Fe_{0.8}CoO_x$) is also shown in Fig. 4 for comparison. In an oxygen-rich atmosphere (20% O_2) the SFC-1 was a cubic perovskite. However, once the pO_2 dropped below 5%, the cubic phase transformed to an oxygen-vacancy-ordered phase. A comparison of Figs. 3 and 4 shows that new peaks appeared in XRD pattern in SFC-1, but not in SFC-2. It is important to note that SFC-1 (see Fig. 4) expanded substantially after phase transition, as can be seen from the change in position of the Bragg peak near 32°. Evidently, this peak in the oxygen-vacancy-ordered phase (in 1% O_2) shifted to the low-angle (larger d-spacing) side of the corresponding peak in the cubic perovskite phase (in 20% O_2).

Thermogravimetric analysis (TGA) showed that the O_2 content x of SFC-1 in 1% O_2 was ≈0.1 lower than that in a sample in 20% O_2 [18]. A comparison of lattice parameters showed that the volume of the primitive perovskite cell V_p is 57.51 A^3 for x = 2.48. These results show that this material (SFC-1) expands as oxygen is removed. Such behavior suggests that an electronic effect is predominant in influencing the specific volume; otherwise, a simple size effect would cause the lattice to shrink. By linear interpolation of these results, we predict that a decrease in x of 0.1 will result in an increase of ≈2% in V_p.

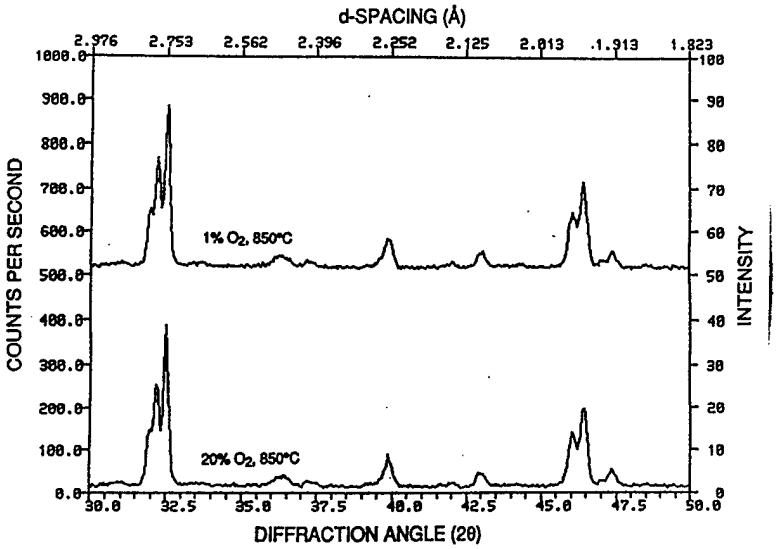

Fig. 3. XRD of SFC-2 at 850°C in 1 and 20% O_2.

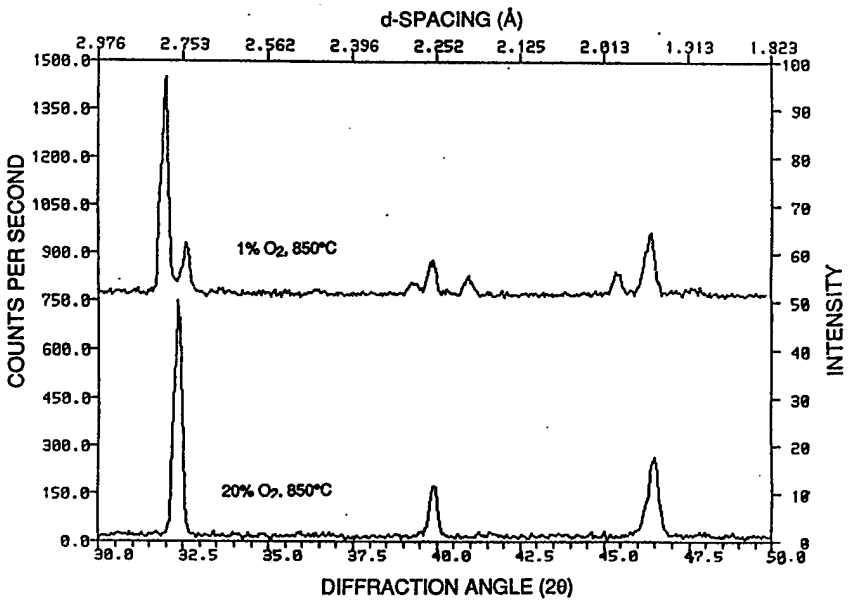

Fig. 4. XRD of SFC-1 at 850°C in 1 and 20% O_2.

Based on the XRD results and the previous TGA data [18], a better understanding of the state of the SFC-1 membrane tube under reaction conditions can be obtained. When the membrane is used as an oxygen separator, high oxygen pressure is maintained inside the tube and low oxygen pressure is maintained outside the tube. Before the tube is heated to high temperature, oxygen distribution in the tube is uniform. Upon heating, the tube begins to lose oxygen that was incorporated during the fabrication. Moreover, the material on the outer wall loses more oxygen than that on the inner wall. As a result, a stable oxygen gradient is generated between the outer and

inner walls. It follows that the material, depending on its location in the tube, may contain different phase constituents. It is probable that the outer zone, with less oxygen, contains more ordered oxygen vacancies and is therefore less oxygen-permeable.

The most significant factor, one that can cause tube fracture, appears to be lattice mismatch between the materials on the inner and outer walls of the tube. The difference in composition between the inner and outer zones leads to an expansion of 2%, which is equivalent to the thermal expansion caused by a 333°C temperature increase.

In contrast to the behavior of SFC-1, SFC-2 exhibited remarkable structural stability at high temperature (Fig. 3). No phase transition was observed as pO_2 was changed. Furthermore, the Bragg peaks stayed at the same position regardless of the oxygen pressure of the atmosphere. This structural stability of SFC-2 is reflected in its physical and mechanical properties, as shown in Table 1. In all cases, SFC-2 shows adequate strength and fracture toughness. Tubes made of this material, unlike those made of SFC-1, were used for methane-conversion reactions to produce syngas without any cracking problem even after operating for hundreds of hours.

Table 1. Physical and mechanical properties of SFC-2 membrane material

Property	Value
Bulk density, $g \cdot cm^{-3}$	4.81
Percent of theoretical density	93
Coefficient of thermal expansion	14×10^{-6}/°C (200-800°C)
Flexural strength, MPa	120.4
Fracture toughness, MPa $m^{1/2}$	2.04
Young's modulus, GPa	124
Shear modulus, GPa	48
Poisson ratio	0.3

Generation of syngas is demonstrated in Fig. 5, showing conversion data obtained with an SFC-2 membrane tube and Rh catalyst at 850°C for ≈70 h. As shown, methane conversion efficiency is >98%, and CO selectivity is 90%. Selectivity is defined here as the percent component produced per feed converted. Measured H_2 yield is approximately twice that of CO, as expected for partial oxidation of methane.

The role of the catalyst in the transport of oxygen flux averaged over the entire SFC-2 tube was tested without the reforming catalyst. The results from a run of ≈350 h are shown in Fig. 6; feed gases are the same as before. In the absence of a catalyst, the oxygen that was transported through the membrane reacted with methane and formed CO_2 and H_2O. Methane conversion efficiency was ≈35% and CO_2 selectivity was ≈90%. Under our operating conditions, measured oxygen flux was ≈ 0.3 std $cm^3.cm^{-2}.min^{-1}$.

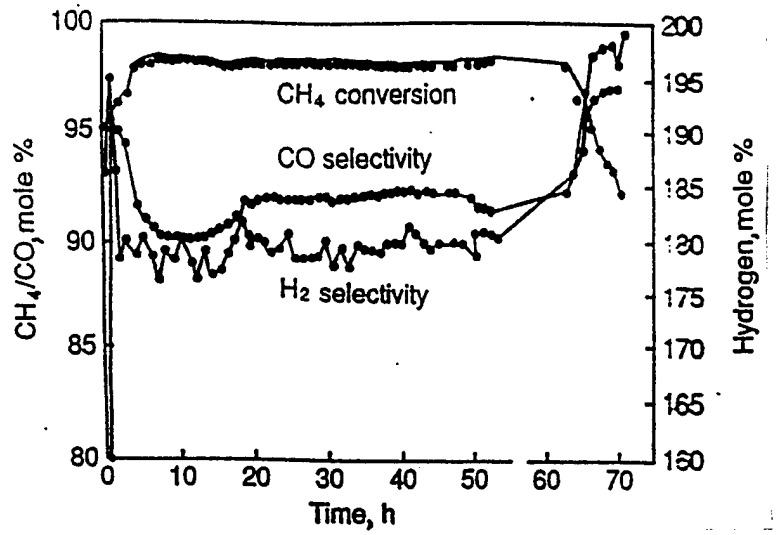

Fig. 5. Methane conversion and CO and H_2 selectivities in SFC-2 membrane reactor with reforming catalyst. Conditions: feed (80% methane, 20% argon) flow, 2.5 cm^3/min; temp., 850°C; pressure 1 atm, membrane surface area, 10 cm^2.

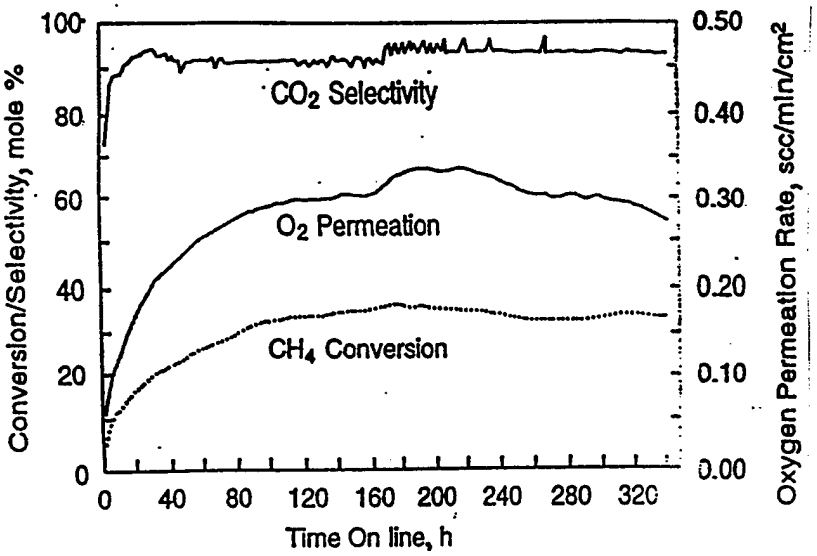

Fig. 6. Methane conversion and CO_2 selectivity and O_2 permeation in SFC-2 membrane reactor without reforming catalyst. Conditions: same as in Fig. 5.

Figure 7 shows the results from a reactor run made under more severe conditions and in the presence of the Rh based catalyst for >500 h. Conversion and selectivities are similar to those of the 350-h run but the oxygen flux was one order of magnitude greater. Some slight deactivation in oxygen permeation rate was observed.

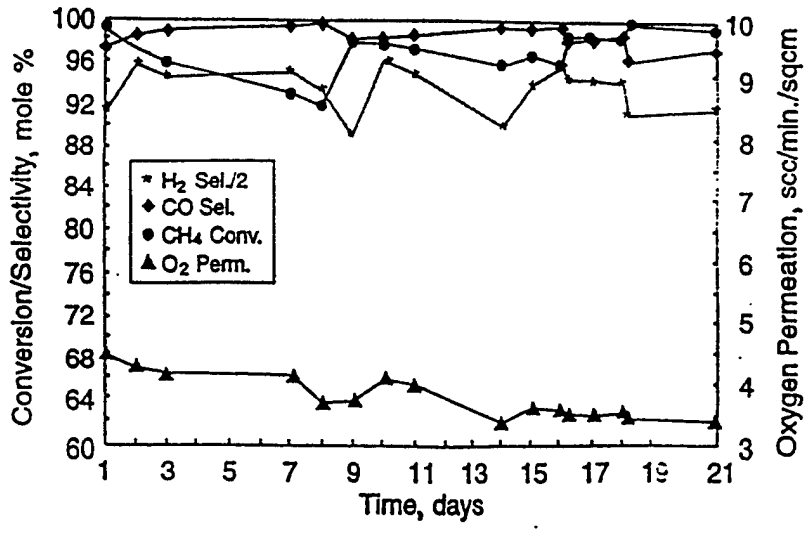

Fig. 7. Methane conversion and CO and H_2 selectivities and O_2 permeation in SFC-2 membrane reactor with reforming catalyst. Conditions: feed, 80% CH_4, 20% Ar; flow, 20 cm^3/min; T = 900°C; pressure 1 atm; membrane surface area, 8 cm^2.

Further confirmation of the stability of this membrane tube is shown in Fig. 8, which shows reactor results over a period of 1000 h. The feed during this period was a typical mixture expected in a commercial recycling feed, namely methane, CO, CO_2, and H_2. Throughout the run, methane conversion was high. A small decline in oxygen permeation was observed. However, this high oxygen flux is consistent with the high diffusion coefficient of 9×10^{-7} $cm^2.s^{-1}$ that was measured at 900°C by the conductivity relaxation method [13] and is also consistent with the diffusion coefficient deduced from the results of reactor experiments [19].

By using the conventional four-probe method and the electron-blocking four-probe method, we measured the total and ionic conductivities directly for SFC-2. Electronic conductivity can then be deduced by subtracting ionic conductivity from total conductivity. The results show that the ratio of ionic to electronic conductivity for SFC-2 is unique in the sense that it is close to unity, unlike other mixed oxides in which there is a preponderance of one value over another.

Oxygen permeability has also been deduced from conductivity data obtained as a function of pO_2 [16]. Oxygen permeability JO_2 is related to total conductivity and ionic transference number of the sample by

$$jO_2 = \frac{RT}{16F^2L} \int_{pO_2^I}^{pO_2^{II}} \sigma_t t_i (1 - t_i) d\ln(pO_2), \qquad (1)$$

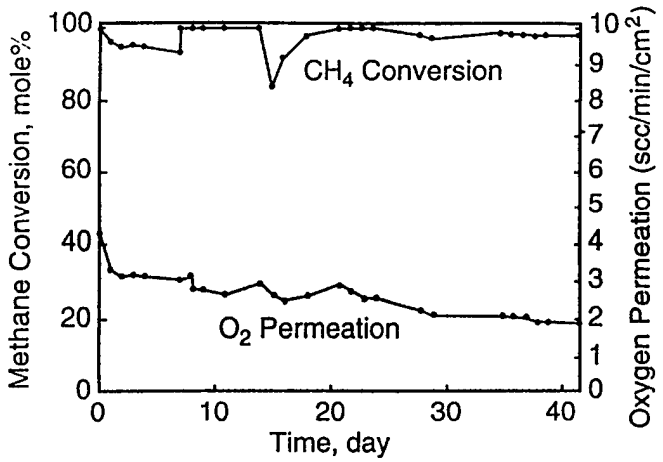

Fig. 8.
Methane conversion and oxygen flux for mixed feed. Conditions: T = 900°C; pressure 1 atm; catalyst 1.5 g; membrane surface area, 8.4 cm^2.

where R is gas constant, T is the temperature in K, L is thickness of the sample, F is the Faraday constant, σ_t is total conductivity, and t_i is transference of oxygen ions. Thus, from conductivity data obtained as a function of pO_2, oxygen permeability can be calculated by Eq.1.

Oxygen permeability of the sample was also determined by using the gas-tight electrochemical cell described earlier [17]. The pO_2 inside the gas-tight electrochemical cell is obtained from

$$pO_2^{II} = pO_2^{I} \exp\left(\frac{4FE}{RT}\right), \tag{2}$$

where pO_2^{II} and pO_2^{I} are the oxygen partial pressures inside and outside the gas-tight cell, respectively, and E is the electromotive force on the sensor electrodes. Under steady-state conditions, the amount of oxygen that enters the cell (by permeation through the specimen disk) must be equal to that pumped out by the YSZ oxygen pump. Therefore, the flow of oxygen through the specimen can be determined by the current applied to the YSZ oxygen pump. Oxygen permeability is related to the current I by

$$JO_2 = \frac{I}{4FS}, \tag{3}$$

where S is the effective cross-sectional area of the specimen disk.

Oxygen permeability obtained from experimental data and Eq. 3 for steady-state pumping current I and geometric parameters of the specimen disk is plotted as a function of $\Delta \log pO_2$ (Fig. 9). $\Delta \log pO_2$ is the logarithmic difference between air (reference) on one side and the lower oxygen pressure on the other side of the specimen disk. Figure 9 shows that JO_2 increases dramatically in the range between 0.21 and 10^{-3} atm, and its slope becomes flatter when pO_2 inside the electrochemical cell is lowered further. Results on oxygen permeability at different oxygen pressure gradients and temperatures show that JO_2 increases with temperature and oxygen pressure gradients, as expected.

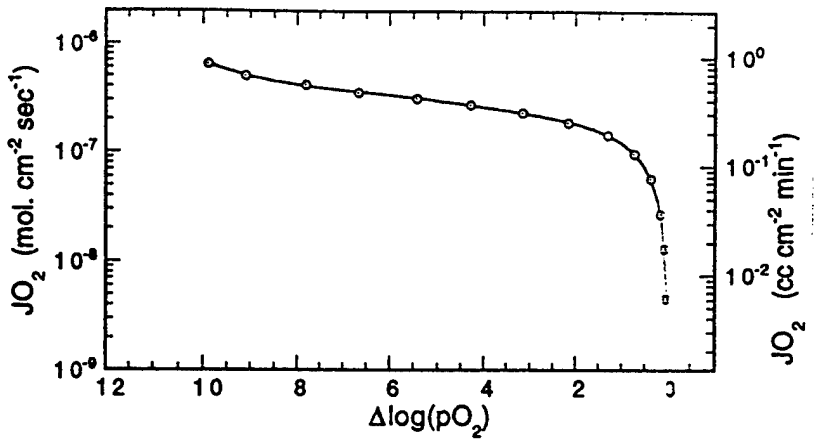

Fig. 9. Oxygen flux as a function of oxygen pressure gradient at 850°C. Specimen thickness = 2.9 mm.

Figure 10 shows oxygen permeabilities (as functions of temperature) determined from our reactor experiments, permeability calculated from conductivity data, and permeability determined from out-of-reactor experiments in a gas-tight electrochemical cell (where the specimen disk is subjected to oxygen pressure gradients). Results from the independent measurements agree within a factor of 2-3. In these measurements, oxygen permeability increased with a decrease in thickness, suggesting that oxygen transport is controlled by bulk rather than surface properties.

5. Conclusions

Mixed-conducting ceramic material of the composition $SrFeCo_{0.5}O_x$ (nonperovskite) has been developed. Extruded and sintered ceramic membrane tubes have performed well in a methane-conversion reactor at 850-900°C for >1000 h with excellent methane conversion efficiency (>98%) and good CO selectivity (≈90%). Stability of this material in methane-conversion reactors relative to that of perovskite-type mixed oxides is consistent with the X-ray diffraction results and various properties we have reported. This material offers feasibility of economically producing syngas on a commercial scale without the use of external electrodes. The high oxygen permeability measured in an operating reactor is consistent with the high oxygen ion diffusivity seen in the conductivity relaxation method and has been confirmed by two other independent measurements, namely permeability calculated from conductivity data at different oxygen partial pressures and from electrochemical measurements on specimen disks exposed to different oxygen pressure gradients in a cell.

Acknowledgments

We are grateful to M. S. Kleefisch and C. A. Udovich of Amoco Exploration and Production for their assistance with the reactor experiments. This work was supported by the U.S. Department of Energy, Federal Energy Technology Center, under Contract W-31-109-Eng-38.

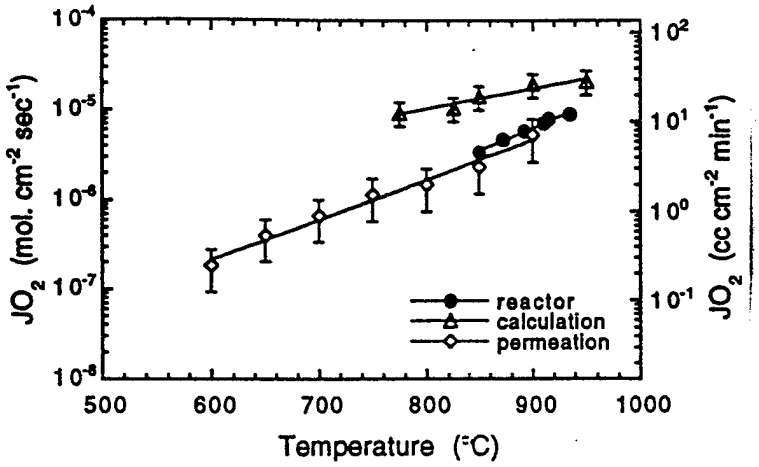

Fig. 10. Oxygen flux determined by three methods (methane conversion reactor experiments, out-of-reactor experiments in an electrochemical cell, and calculated from conductivity data vs. temperature for SFC-2.

References

1. H. D. Gesser and N. R. Hunter, Chem. Rev., 85 (1985) 235.
2. N. D. Spenser and C. J. Pereiva, J. Catal., 116 (1989) 399.
3. Y. Amenomiya, V. I. Buss, M. Goledzinszka, and A. R. Sanger, Catal. Rev. Sci. Eng., 32 (1990) 163.
4. G. Henrici-Olive and S. Olive, Angew. Chem. Int. Ed. Engl., 15 (1976) 136.
5. Y. Teraoka, H. M. Zhang, S. Furukawa, and N. Yamozoe, Chem. Lett. (1985) 1743.
6. Y. Teraoka, T. Nobunaga, and N. Yamazoe, Chem. Lett. (1988) 503.
7. Y. Teraoka, H. M. Zhang, K. Okamoto, and N. Yamazoe, Mater. Res. Bull., 23 (1988) 51.
8. U. Balachandran, S. L. Morissette, J. J. Picciolo, J. T. Dusek, R. B. Poeppel, S. Pei, M. S. Kleefisch, R. L. Mieville, T. P. Kobylinski, and C. A. Udovich, Proc. Int. Gas Research Conf., ed., H. A. Thompson, Government Institutes, Inc., Rockville, MD (1992) 565.
9. K. J. Mazanec, T. L. Cable, and J. G. Frye, Jr., Solid State Ionics, 53 (1992) 111.
10. K. Nisancioglu and T. M. Gur, Solid State Ionics, 72 (1994) 199.
11. H. Kruidhof, H. J. M. Bouwmeester, R. H. E. Doorn, and A. J. Burggraf, Solid State Ionics, 63 (1993) 816.
12. U. Balachandran, J. T. Dusek, S. M. Sweeney, R. B. Poeppel, R. L. Mieville, P. S. Maiya, M. S. Kleefisch, S. Pei, T. P. Kobylinski, C. A. Udovich, and A. C. Bose, Am. Ceram. Soc. Bull., 74 (1995) 71.

13. B. Ma, U. Balachandran, J. H. Park, and C. U. Segre, Solid State Ionics, 83 (1996) 65-71.

14. W. F. Brown, Jr., and J. E. Strawley, ASTM STP 410, Philadelphia, PA (1967).

15. J. Krautkramer and H. Krautkramer, Ultrasonic Testing of Materials, Springer-Verlag, Berlin (1983).

16. B. Ma, U. Balachandran, and J. H. Park, J. Electro. Soc. 143(5) (1996) 1736.

17. B. Ma, U. Balachandran, C. C. Chao, and J. H. Park, to be published in Ceramic Transactions Series of the American Ceramic Society.

18. S. Pei, M. S. Kleefisch, T. P. Kobylinski, J. Faber, C. A. Udovich, V. Zhang-McCoy, B. Dabrowski, U. Balachandran, R. L. Mieville, and R.B. Poeppel, Catalysis Lett., 30 (1995) 201.

19. P. S. Maiya, M. S. Kleefisch, J. T. Dusek, R. L. Mieville, U. Balachandran and C. A. Udovich, presented at 1st Int. Conf. on Ceramic Membranes, 188th Mtg. of Electrochemical Soc. Inc., Chicago, October 8-13, 1995; to be published in Solid State Ionics.

Report Number (14) ANL/ET/CP--93360
CONF-9705250--

Publ. Date (11) 199704
Sponsor Code (18) DOE/EE, XF
JC Category (19) UC-1406, DOE/ER

DOE